THE JOURNAL OF PHYSICAL CHEMISTRY B
A JOURNAL OF THE AMERICAN CHEMICAL SOCIETY

pubs.acs.org/JPCB Article

Molecular Dynamics Simulations of Soft and Reactive Landing of Proteins Desorbed by Argon Cluster Bombardment

Samuel Bertolini* and Arnaud Delcorte

Cite This: https://doi.org/10.1021/acs.jpcb.4c01698 Read Online

ACCESS | Metrics & More | Article Recommendations | Supporting Information

ABSTRACT: Reactive molecular dynamics (MD) simulations were conducted to investigate the soft and reactive landing of hyperthermal velocity proteins transferred to a vacuum using large argon clusters. Experimentally, the interaction of argon cluster ion beams ($Ar_{1000-5000}^{+}$) with a target biofilm was previously used in such a manner to transfer lysozymes onto a collector with the retention of their bioactivity, paving the way to a new solvent-free method for complex biosurface nanofabrication. However, the experiments did not give access to a microscopic view of the interactions needed for their full understanding, which can be provided by the MD model. Our reactive force field simulations clarify the landing mechanisms of the lysozymes and their fragments on collectors with different natures (gold- and hydrogen-terminated graphite). The results highlight the conditions of soft and reactive landing on rigid surfaces, the effects of the protein structure, energy, and incidence angle before landing, and the adhesion forces with the collector substrate. Many of the obtained results can be generalized to other soft and reactive landing approaches used for biomolecules such as electrospray ionization and matrix-assisted laser desorption ionization.

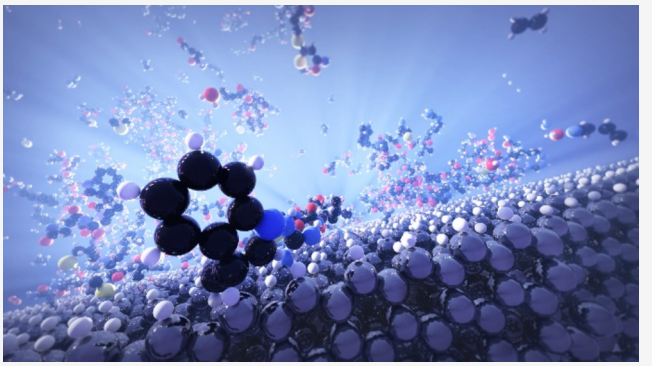

1. INTRODUCTION

The advancement and industrial development of biosensors, biocatalysts, bioanalytical tools, and drug delivery systems often require the enhancement of immobilization and preservation of protein bioactivity on a surface.[1−4] While these proteins can be deposited using solution-based techniques, their specific affinity with the surface or charge accumulation, often leads to diminished bioactivity and limits their deposition to a singular layer.[5,6] The adsorption process is strongly surface-dependent and the subsequent drying process may also interfere with the production of uniform layers.[7−9] Achieving more complex multilayer assemblies necessitates binding the proteins in a step-by-step process utilizing polyelectrolytes,[10,11] covalently coupling the proteins or using ligands.[12−14]

Alternatively, within the realm of mass spectrometry methods, beyond their primary role in the analysis and identification of biomolecules, lies the capacity to deposit proteins onto a surface under vacuum conditions[15] using a technique known as ion soft landing (SL). Protein ion SL can be executed using various methods, such as electrospray ionization (ESI) and matrix-assisted laser desorption ionization (MALDI), both able to produce large molecular ions that are then mass-selected and guided to a collector surface with a lateral resolution defined by the beam focus.[16−18] Cooks et al.[19] have categorized the processes of collision and landing. Here, we emphasize SL as the deposition of molecules/clusters without surface reaction, reactive landing (RL)[20,21] as the deposition involving surface reactions, and surface-induced dissociation (SID) as the process where collisions induce fragmentation upon molecule/cluster landing. In the landing process, the translational velocity of the molecules colliding on the surface is distributed as internal energy, which can induce local unfolding, disorder, and reactions.[22] The landing efficiency minimally depends on the proteins' charge states, instead, the landing energy and type of surface are critical for fragmentation to occur.[23] The simple acceleration of a molecule onto a surface can induce a nonselective reaction[24] and the energy transferred from the collision can produce further reaction on the surface.[25] Alternatively, different molecule orientations in the collision can induce diverse reaction pathways.[26] Molecule orientation can be guided using optical[27] or hexapole fields.[28] In addition, conformation and reaction stability of proteins can be improved by cryo methods, that reduce thermal diffusion and structure fluctuations.[29,30]

Received: March 14, 2024
Revised: June 7, 2024
Accepted: June 18, 2024

During the ion SL process, charges accumulate on the surface over extended periods of time, a phenomenon that can be mitigated through electron transfer or proton migration. Despite the presence of charges, the proteins' bioactivity may remain intact, plausibly due to inherent refolding mechanisms.[31−34] Remarkably, the proteins' folded structures can endure even after SL, notwithstanding the loss of attached water molecules.[35,36] Increasing the collision energy and/or the proteins' landing temperature typically induces protein fragmentation (SID) and reactions with the substrate (RL).[37−39]

A novel method known as the iBEAM technique[40,41] has emerged as an innovative approach for the soft landing of proteins irrespective of their charge state, employing large kiloelectronvolt argon gas cluster ion beams (GCIB) to transfer proteins in a manner akin to SIMS. Compared to sample sputtering by isoenergetic atomic and small cluster ions, protein desorption through iBEAM is characterized by inducing minimal damage to the molecules and has showcased its ability to transfer bioactive lysozymes (14 kDa) from a source (target) to a recipient surface (collector).[41] Moreover, it has demonstrated precision in constructing multilayered structures at the nanoscale,[42] while computational simulations indicated promising prospects for the successful transfer of even larger proteins, such as glucose oxidase (64 kDa).[43] Notably, the extent of protein damage during desorption depends significantly on the kinetic energy per atom (E/n) of the GCIB, with considerable reduction in internal energy (thereby fragmentation) observed for E/n values smaller than 2 eV/atom.[42,44] However, our simulations also accentuated the role of cluster size (i.e., the number of nuclei n) as a secondary factor in exacerbating fragmentation at constant E/n.[45] Given its lineage from SIMS, efforts to further limit fragmentation through the application of cryogenic methods might also be promising for iBEAM soft landing.[46,47]

Computer simulations offer a distinctive advantage by facilitating an understanding of fundamental concepts that are either prohibitively expensive or unfeasible to explore solely through experimental means, particularly within the domains of sputtering and desorption[48−51] but also molecular landing. Various methodologies, encompassing quantum mechanics (QM), molecular mechanics (MM), and QM/MM approaches, have been employed to simulate the intricacies of SL and RL. In the context of SL, these simulations explored the modifications in the structural features of proteins and peptides across diverse substrates subsequent to the landing event.[52,53] The configurations, or the entropies associated with the peptide's configurations, are particularly dependent on whether the initial structures are helical or globular.[54] The sticking efficiency of landing peptides exhibits a dependence on collision energy, which, in turn, may be dependent on the collision angle. The process of landing can induce reactions by augmenting vibrational energy and instigating fragmentation along diverse pathways.[55−59] Notably, the reactivity of peptides is amplified in the presence of neutral species, and their fragmentation is intricately linked to proton transfers, with oxygen and nitrogen emerging as the principal sites for transfer. The RL efficiency is also dependent on the terminal groups of the surface,[60,61] while the particular side chains of the peptides also directly influence the RL efficiency. For example, a lysine shows more efficiency to react than an RGDGG side chain.[62] Investigating RL simulations, a delineation of the structural characteristics of deposited films unfolds, elucidating the polymerization of deposited molecules and the generation of amorphous carbon materials during the landing process.[63−66] Less computer intensive than QM methods (DFT), classical molecular dynamics (MD) using chemical reactive force fields (Brenner, COMB, AIREBO, ReaxFF) appears to be the method of choice to study soft and reactive landing (and the transition between the two) for large systems, long times, or repeated impact simulations. In particular, the implementation of ReaxFF[67−69] has emerged as a fitting methodology for investigating protein SL and RL, having been effectively employed in studying various phenomena, such as the fragmentation of polymer surfaces during cluster collisions[70] or the sputtering of amino acids by GCIB from bulk solids and from graphite substrates.[71,72] Additionally, recent enhancements in the ReaxFF code display promising advancements by enabling explicit simulation of electrons and accelerating the computation of charges.[73−76]

Recently, ReaxFF simulations focusing on the desorption of lysozymes (Lyz) and glucose oxidase (GOx) from a gold substrate were conducted in our group, revealing the potential for intact protein desorption and the dependence of fragmentation on the bombardment conditions.[43,45] An important aspect of those investigations was to shed light on the difference in molecular desorption from gold, producing proteins with high internal energies, prone to fragmentation, and desorption from a protein matrix, leading to the emission of (clusters of) proteins with comparatively lower internal energies, even with minimal denaturation. Incidentally, our simulations highlighted intriguing aspects of reactivity, such as the formation of Au−S and H−S bonds attributed to the presence of cysteine amino acids, mirroring experimental observations.[77,78] The present study capitalizes on these results to delve into the investigation of lysozyme soft and reactive landing, examining diverse scattering angles and protein configurations obtained from our previous desorption simulations in order to elucidate the influence of these variables on the landing process. Moreover, we explore two different substrates; gold and hydrogen-terminated graphite (HTG) serve as examples of rigid surfaces, where electrostatic and van der Waals interactions govern the interactions with the landing protein.

2. COMPUTATIONAL METHODS

The soft landing of lysozymes on a substrate was achieved through the utilization of the large-scale atomic/molecular massively parallel simulator (LAMMPS) code, employing reactive force fields (ReaxFF).[79−81] The characteristics of the proteins used in these soft and reactive landing simulations were derived from a prior study involving the desorption of lysozyme by large argon clusters,[45] employing the same force field.[82−84] These lysozyme proteins were categorized into three groups: isolated (Figure 1A), cluster (Figure 1B), and fragment (Figure 1C). The clusters of lysozymes were desorbed from a lysozyme bilayer situated on top of a gold substrate; in this case, the clusters contained 5 and 3 lysozymes each. In contrast, the isolated lysozymes were desorbed from a gold substrate by various-sized argon clusters with low-impact kinetic energy, so that each system desorbed a single lysozyme (see Table S1). As the desorption of lysozyme can be correlated with the experimental parameters of iBEAM (Ar clusters size and velocity or protein layer thickness), here the simulations of landing can be directly correlated with the previous output.[45] The fragments consisted of amino acid

https://doi.org/10.1021/acs.jpcb.4c01698
J. Phys. Chem. B XXXX, XXX, XXX−XXX

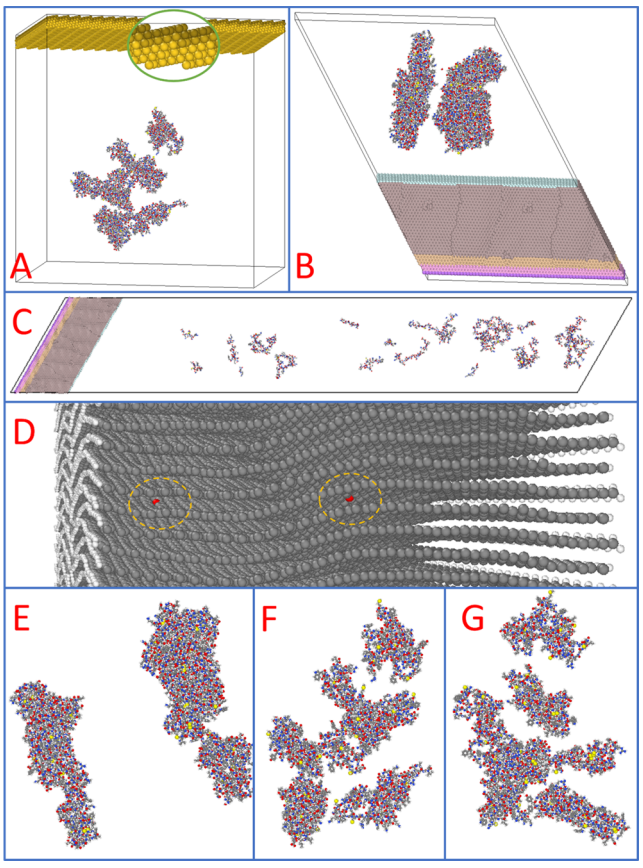

Figure 1. Configuration of the unit cells used to simulate soft landing. (A) Gold surface and isolated proteins. (B) Graphite (HTG) surface and clustered proteins. (C) HTG surface and large fragments. (D) Examples of carbon atoms removed (red) from the graphite to create defects. (E) Highlighted structure of the protein cluster. (F, G) Highlighted structures of the isolated proteins showing different points of view. The damping and frozen layers on gold have a darker contrast, and the frozen layer is darker than the damping layer. On graphite, the frozen atoms have a purple color for H and pink for C, while the damping C atoms have an orange color.

chain segments desorbed from gold with argon clusters having high impact kinetic energy (>2 eV/atom). All simulations were conducted with a time step of 0.1 fs, employing the NVE (microcanonical) ensemble, over a total simulation duration of 150 ps. Here, although the settings are NVE ensembles, the Langevin thermostat applied at the bottom of the slabs will drag the energy of the system, transferred through phonons interaction.

The translational and (internal) kinetic energy per unit mass and the translational velocity of each cluster and isolated lysozymes are reported in Table 1. Calculating the energy per mass, it is possible to compare various protein structures, since different systems can exhibit small or large differences in terms of atom numbers and element types. The small difference in the total mass of lysozymes is due to the loss of water embedded in the structure and/or H atoms upon desorption. For the simulations of soft and reactive landing, the internal energy was preserved while the direction of the translational velocity vectors was adjusted to enable collisions with the substrate at various angles, while keeping the vector's magnitude constant. To redirect the translational velocity of each protein and cluster, the center-of-mass velocity of the ensemble was subtracted from each atom's velocity, and a new

Table 1. Energies and Velocities of the Lysozyme Clusters, Isolated Proteins, and Group of Fragments

reference	mass (Da)	translational energy (eV/Da)	internal energy[a] (eV/Da)	translational velocity (Å/fs)
cluster 1	42 966	0.63×10^{-2}	1.14×10^{-2}	1.10×10^{-2}
cluster 2	71 681	0.31×10^{-2}	1.06×10^{-2}	0.77×10^{-2}
isolated 1	14 297	1.55×10^{-2}	1.35×10^{-2}	1.72×10^{-2}
isolated 2	14 296	1.26×10^{-2}	1.45×10^{-2}	1.55×10^{-2}
isolated 3	14 297	3.01×10^{-2}	2.04×10^{-2}	2.40×10^{-2}
isolated 4	14 297	2.33×10^{-2}	1.44×10^{-2}	2.11×10^{-2}
isolated 5	14 266	2.99×10^{-2}	1.93×10^{-2}	2.39×10^{-2}
isolated 6	14 265	2.32×10^{-2}	1.84×10^{-2}	2.10×10^{-2}
fragment 1	13 087	2.31×10^{-2}	2.23×10^{-2}	2.10×10^{-2}
fragment 2	9438	3.20×10^{-2}	2.59×10^{-2}	2.47×10^{-2}
fragment 3	13 883	6.81×10^{-2}	2.45×10^{-2}	3.61×10^{-2}
fragment 4	9135	9.04×10^{-2}	2.84×10^{-2}	4.16×10^{-2}
fragment 5	4515	12.18×10^{-2}	3.26×10^{-2}	4.82×10^{-2}
fragment 6	11 770	8.65×10^{-2}	2.35×10^{-2}	4.07×10^{-2}
fragment 7	9435	12.04×10^{-2}	3.09×10^{-2}	4.80×10^{-2}
fragment 8	4723	17.38×10^{-2}	4.31×10^{-2}	5.76×10^{-2}

[a]Internal energy contains only rotation and vibration kinetic energies. All the energies are divided by the total mass.

velocity vector with the same modulus but a selected direction was added. When the collision angle between the substrate's plane and the protein's translational velocity vector reaches 90°, it is referred to as a "normal landing", and angles other than 90° are termed "oblique landings".

Finally, three distinct substrates were examined under the conditions of periodic boundaries in all directions: gold, H-terminated graphite (HTG), and defective H-terminated graphite (defects on the basal plane), where after equilibration at 300 K, the same positions and velocities were replicated to build the systems. The gold substrate possesses dimensions of 239.8 × 247.2 Å^2, featuring cleavage along the <543> direction, with one frozen layer, one Langevin damping layer at 300 K, and 100 steps of damping factor. It also incorporates 3 layers of free gold atoms for a total thickness of 12 Å (Figure 1A). The HTG substrate is terminated with hydrogen atoms and comprises various graphene layers on its surface, with an area of 136.9 × 108.6 Å^2 and a thickness of 77.1 Å. In this setup, one hydrogen-terminated region is held fixed alongside one aromatic sequence, while two aromatic sequences serve as a damping Langevin region at 300 K with 100 steps factor, both regions set at the slab's bottom. The remaining part of graphite remains free (Figure 1B). The large vacuum region that separates the slabs and their thickness guarantee a negligible interaction between the top and bottom layers, and it also assures that phenomena occurring in the top layers (landing) do not interact with ones in the bottom of the slab (landing of backscattered molecules). Defects are an intrinsic property present in graphite; here, they were introduced by randomly removing two carbon atoms from each graphite layer far away from each other (Figure 1D), therefore guaranteeing that proteins land over a defective layer. Due to the periodicity of the cell, the vacuum separates the bottom and the top surface by a size of 238 and 143 Å in the gold and HTG slabs, respectively. Furthermore, Table 2 provides a summary of the substrates, protein structures, and incident angles with respect to the surface plane used in the study.

The adsorption energies were calculated by the difference between the initial and final average energy of the relaxed

https://doi.org/10.1021/acs.jpcb.4c01698
J. Phys. Chem. B XXXX, XXX, XXX−XXX

Table 2. Configuration of the Computed Systems Including the Substrate Nature, the Structure of the Proteins, and the Incidence Angle

substrate	protein structure	incident angle
gold	cluster	90°
gold	isolated	90°
gold	isolated	30°
HTG	cluster	60°
HTG	isolated	90°
HTG	isolated	60°
HTG	fragments	60°
HTG with defects	cluster	60°

system, comparing the adsorbed protein and the protein in a vacuum, consequently reducing artifacts that could be generated due to the electronegativity equalization method (EEM) when performed by ReaxFF. The adsorption energy using the density functional theory (DFT) method was calculated by optimizing the whole system and the isolated subsystems (slab and protein). In order to reduce computation costs, the DFT simulations used neurotensin instead of lysozyme with a reduced-size slab. The FCC gold cell was cleaved in the <100> direction, with two frozen bottom layers and two free top layers with the protein located on top of the slab for a total size of 19.85 × 19.92 × 37.05 Å^3 (Figure S7A). A similar configuration was used for HTG, represented by two aromatic rings with the bottom two carbon sequences frozen, for a total size of 22.18 × 20.83 × 30.00 Å^3 (Figure S7B). On gold and graphite, neurotensin was randomly added to the system, and the same peptide configuration was equally set for both substrates. Additionally, another orientation was tested on gold. The DFT calculations were performed by Quantum Espresso 7.2 using Perdew−Burke−Ernzerhof (PBE) and Projector-Augmented Wave (PAW) with an energy cutoff of 60 Ry, γ points and further standard values.[85,86] The charges were calculated using Bader charge.[87] The methodology for amino acid (AA) identification and color type sequence is described in the Supporting Information.

In every figure, the atoms are colored by type or by sequence. The type color code is H is white, C is gray, N is blue, O is red, S is yellow, and Au is golden; while carbon and hydrogen from the HTG can be colored green and cyan, respectively. The sequence color code is nonidentified amino acid is gray, glycine is white, alanine is red, serine is orange, proline is yellow, valine is green, threonine is blue, cysteine is purple, leucine is pink, isoleucine is brown, asparagine is cyan, aspartic acid is dark green, glutamine is light red, lysine is light orange, glutamic is light yellow, methionine is light green, histidine is light blue, phenylalanine is light purple, arginine is light pink, tyrosine is light brown, and tryptophan is light cyan.

3. RESULTS

3.1. Landing on Gold. One question that arises during the landing of a protein on a collector is whether the process is reactive. To investigate the potential damage caused by the landing to the protein, we monitored the number of species over time as a measure of protein fragmentation, which increases as more species form. The number of species formed upon the impact of lysozyme clusters on gold remains relatively constant over time (Figure 2A). In contrast, for the group of isolated proteins, the number of species increases monotonically during the landing and the number of produced fragments depends on the angle (normal or oblique) with which the proteins collide with the gold substrate (Figure 2A). Initially, the normal impact induces a faster increase in the number of species because of the shorter distance traveled by the protein compared to the oblique impact. In the normal impact, the number varies from 15 to 40 species at the end of the collision, while in the oblique impact, it reaches 48 species. However, after the end of the collision phase, the rate of fragmentation continues to depend on the angle of impact, with a larger value for the oblique landing. At the end of the trajectory (150 ps), the numbers finally reach ∼50 species for the normal landing and ∼80 species for the oblique landing. The difference in the fragmentation between the cluster and the isolated proteins may be associated with the difference in internal energy and translational velocity, which are higher in the isolated lysozymes. We consider that the translational energy is predominantly affecting fragmentation because it is primarily transformed into internal energy during the collision with the surface. However, a more systematic procedure would be necessary to fully investigate the effect of translational energy on the fragmentation of the proteins.

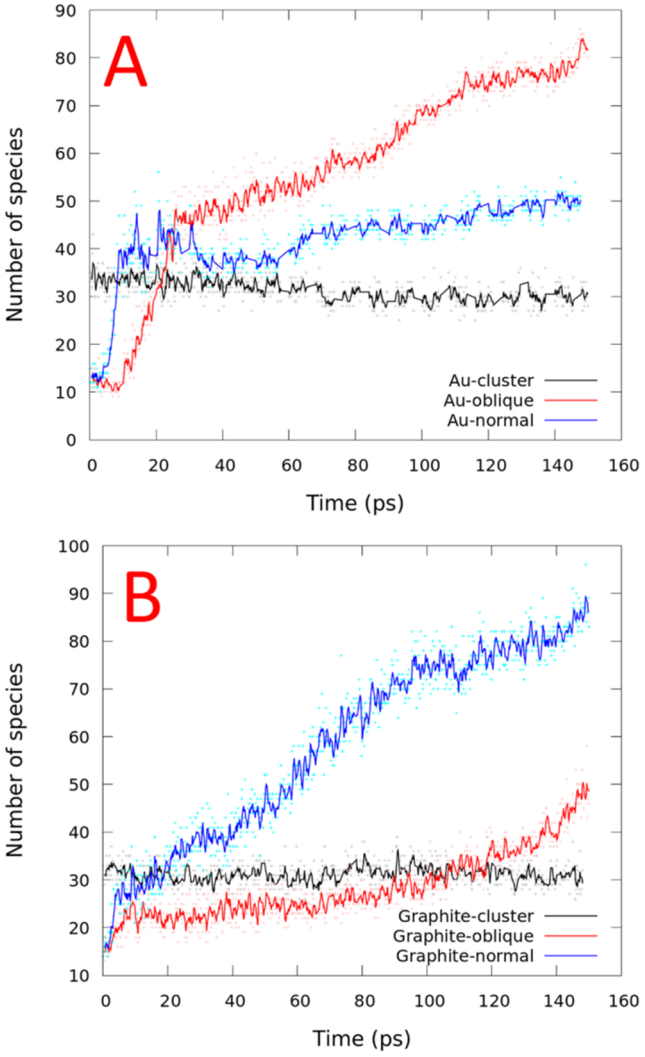

Figure 2. Time evolution of the number of species formed upon landing on (A) gold and (B) H-terminated graphite. Data points are shown in light colors, and the average line is shown in dark colors.

https://doi.org/10.1021/acs.jpcb.4c01698
J. Phys. Chem. B XXXX, XXX, XXX−XXX

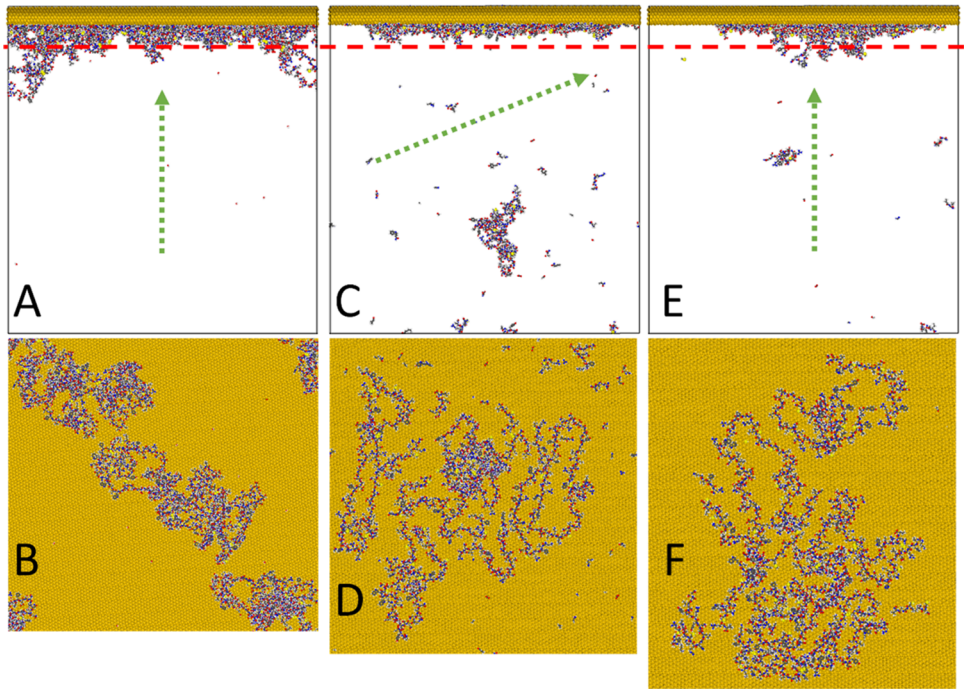

Figure 3. Landing, backscattering, and denaturation on gold for normal collision of protein clusters, (A) front and (B) top view; oblique collision of isolated proteins, (C) front and (D) top view; and normal collision of isolated proteins, (E) front and (F) top view.

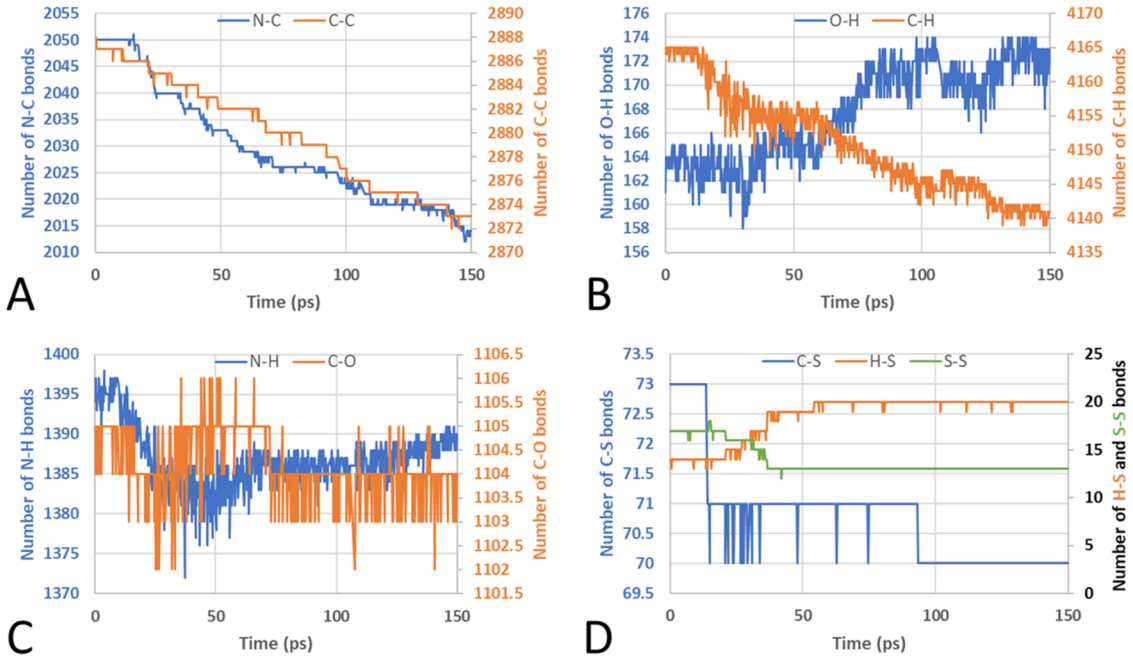

Figure 4. Time evolution of the number of bonds. (A) N−C and C−C bonds, (B) O−H and C−H bonds, (C) N−H and C−O bonds, and (D) C−S, H−S, and S−S bonds.

When the lysozymes come into contact with the gold substrate, they undergo compression and transfer a portion of their kinetic energy to the substrate. Simultaneously, the gold substrate exerts an elastic reaction against the proteins. As a result, portions of the proteins may be backscattered and not adsorbed on the substrate, depending on the protein's initial structure (isolated or clustered). In the case of lysozyme colliding as clusters (Figure 3A,B), the proteins adsorb completely, although certain portions of the protein chains can momentarily reflect and later readsorb onto the substrate. Of note is that the water molecules remaining trapped in the protein cluster structure after desorption are entirely expelled into the vacuum upon impact (Figure S1); therefore, water is eliminated from the lysozyme 3D structures after desorption or landing. The backscattering phenomenon becomes more pronounced when isolated proteins collide with the gold substrate. In those cases, not only water but also fragments are reflected from the surface (Figure 3C−F). The impact angle also affects the behavior of isolated proteins: in oblique landing, more fragments, including large ones, are generated

https://doi.org/10.1021/acs.jpcb.4c01698
J. Phys. Chem. B XXXX, XXX, XXX−XXX

and ejected into the vacuum (Figure 3C) while in normal landing, only small fragments are backscattered (Figure 3E). As a consequence, the growth of the adsorbed protein layer occurs more rapidly when proteins collide as clusters and more slowly when they collide as isolated lysozymes in an oblique collision (Figure 3A−C). Two distinct backscattering mechanisms were observed in the simulations. The first involves fragmentation, where a portion of the protein becomes adsorbed on the gold, while another part of the polymeric chain is cleaved as a result of the intense stress, ejecting fragments into the vacuum. The second mechanism occurs when a lysozyme collides in an area already occupied by a protein, causing it to rebound without undergoing further fragmentation (Figure S2).

The surface-induced dissociation of proteins onto the gold substrate generates chemical changes, primarily due to fragmentation reactions. In the case of protein clusters, the only bonds formed are the O−H bonds. Beyond reaction, this phenomenon can also be attributed to the formation of hydrogen bridges, fluctuations in temperature, and the specified cutoff distance (Table S2) utilized in the calculations. The numbers of other bond types remain relatively constant over time (Figure S3). Variations in the number of bonds are more noticeable in oblique collisions (Figure S3) compared to normal collisions (also illustrated in Figure S3). In the case of oblique collisions, the numbers of bonds associated with the breaking of the protein backbones, namely, N−C and C−C bonds, decrease over time (Figure 4A). The abstraction of hydrogen atoms during the collision and their recombination tend to increase the number of O−H bonds (Figure 4B). In general, the primary source of hydrogen is the breaking of C−H (Figure 4B) and N−H bonds (Figure 4C). However, around 48 ps, the number of N−H bonds begins to increase again, suggesting that C−H bonds are the primary source of hydrogen for forming other hydrogen bonds. The higher amount of C−H bonds compared to N−H bonds could explain why C−H bonds are the main source of hydrogen atoms. With smaller numbers in comparison to other bonds, C−S and S−S bonds tend to break to create S−H bonds (Figure 4D). The C−O bonds experience slight oscillations over time but can generally be considered as remaining constant.

3.2. Landing on H-Terminated Graphite (HTG).

The lysozyme clusters also adsorb on HTG without fragmentation, as measured by the time evolution of the number of species (Figure 2B). The reduced van der Waals interactions between HTG and lysozyme also limit the proteins from spreading across the surface. The resulting arrangement is therefore more condensed than that on gold and resembles the original cluster structure (Figure 5A). Neglecting the variance in the oblique incidence angle between HTG and gold (60° versus 30°), there is an inversion in terms of fragmentation, with the normal collision generating a higher fragmentation ratio than the oblique collision on HTG (Figure 2B). Furthermore, the data suggest that a higher number of fragments can be formed while landing on the HTG substrate (normal impact).

The initial configuration of the system (isolated or cluster, normal or oblique impact) also has an impact on the backscattering from HTG. In our simulations, the reflected molecules and fragments can be captured by an additional layer of graphite, because periodic boundary conditions were used (top of the frames in Figure 5). When the proteins land as clusters, only water is stripped from the lysozymes, but no protein backscattering occurs (Figure 5A). During oblique collisions of isolated proteins on HTG, some of them ricochet into the vacuum, also generating smaller fragments (Figure 5B). However, in parallel with the larger number of fragments generated upon the normal impact of isolated lysozymes, more protein fragments are backscattered compared to oblique landings, as indicated by the more pronounced accumulation on the top graphite layer (Figure 5C). Moreover, after landing, the proteins tend to move across the HTG surface until they equilibrate, which is independent of the collision angle of the protein's initial structure.

In a reactive scenario, three distinct types of reactions are possible: protein fragmentation, protein reaction with the substrate, and protein reaction among themselves. While fragmentation reactions were observed on the gold substrate, lysozymes also engaged in reactions with the graphite substrate. This is exemplified by the formation of an N−C bond following the landing of the protein cluster on HTG

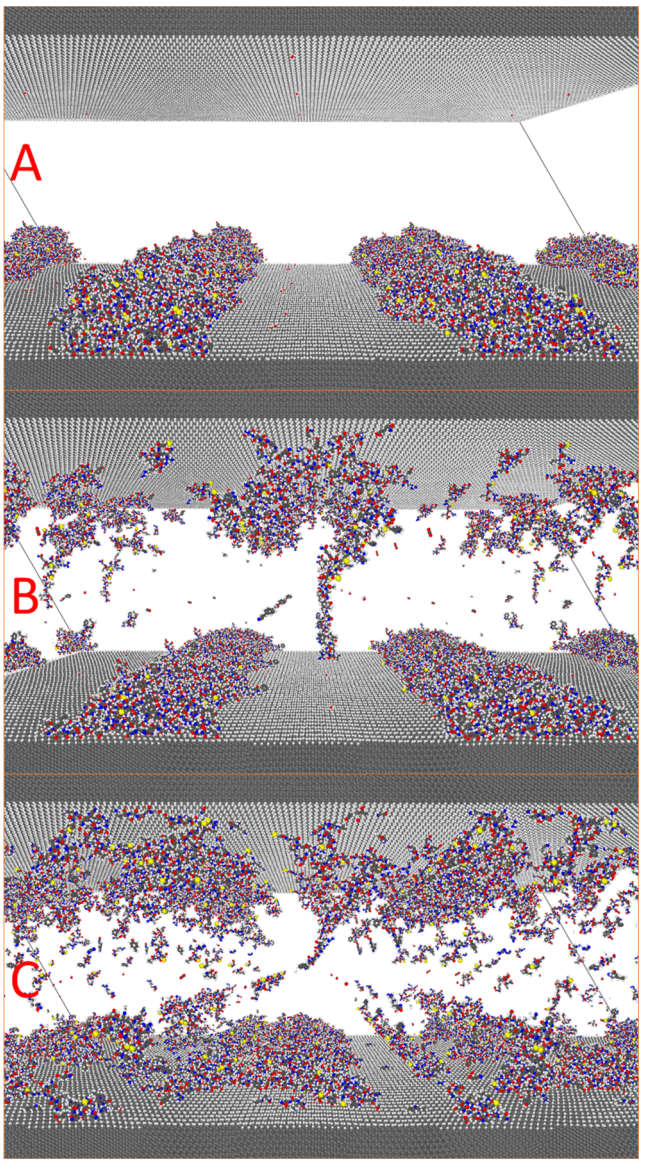

Figure 5. Perspective view of landed and backscattered proteins on HTG (repeated 3 × 3 × 1 times). (A) Landing of protein clusters under normal incidence, (B) landing of isolated proteins under oblique incidence, and (C) landing of isolated proteins under normal incidence.

https://doi.org/10.1021/acs.jpcb.4c01698
J. Phys. Chem. B XXXX, XXX, XXX−XXX

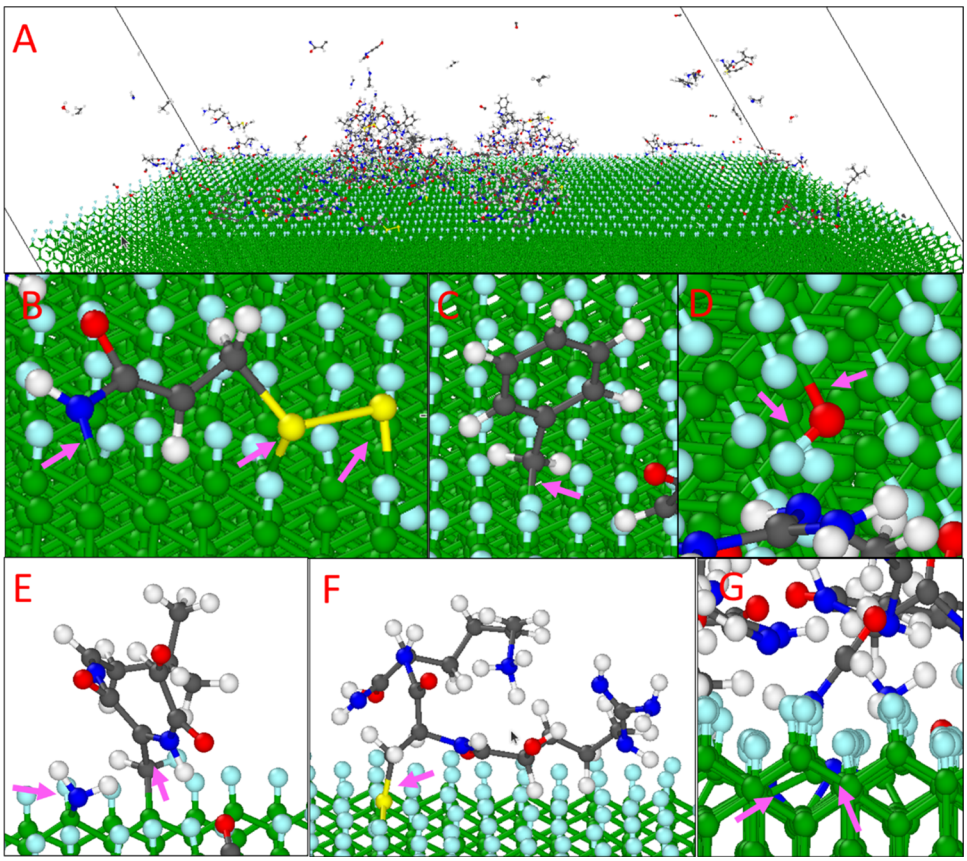

Figure 6. Chemisorption of fragments on HTG. (A) Perspective view of the slab and the chemisorbed fragments; (B−G) examples of fragments chemisorbed at the surface.

(Figure S4A,C,D). In the same context, there is evidence of hydrogen migration from one protein to another, emphasizing the potential for proteins to react with each other. The presence of defects in the HTG surface does not suggest any increase in the reactivity of the slab. As a matter of fact, the clusters did not form any bonds with the defective HTG in our simulations (but this might be a matter of statistics). In addition, fragments from different lysozymes can recombine to form a new molecule, as observed in an aggregate formed upon reflection from the HTG after a normal collision (Figure S4B).

As explained in the Methods Section, the initial state of the lysozyme molecules, clusters, and fragments used for soft and reactive landing or surface-induced dissociation in the current simulations were obtained from previous calculations of large argon cluster impacts on lysozyme molecules and clusters adsorbed on gold.[45] The formation of fragments during the desorption of single lysozymes adsorbed on gold is mainly induced by higher velocity Ar_n cluster impacts (higher E/n) and also by larger Ar_n cluster size (higher n). Consequently, the fragments fly from the target with high translational velocity and internal energy (Table 1). As a result, many of the fragments further break down upon impact with the surface, with some pieces being backscattered in the gas phase while some other parts react with the HTG surface (Figure 6). After reflection, small fragments may decelerate the proteins that have not yet landed on the substrate. The number of reactions increases proportionally to the number of colliding fragments. Although the majority of fragments impinging on the graphite reflect into the gas phase, the likelihood of surface adsorption increases with the mass of the fragment. With time, the fragments accumulate on the surface, resulting in the formation of numerous covalent bonds with the HTG. Diverse types of bonds can be formed with the HTG, for example, C−C, C−N, C−O, and C−S bonds (Figure 6B−G). Small fragments and amino acids chemisorb on the surface, normally bonded by carbon from the substrate; however, hydrogen from the surface can migrate to the fragment landed. Not only chemisorbed but also physisorbed fragments stick to the surface. This is especially valid for larger fragments, which land on the surface with minimal fragmentation. Moreover, some fragments can penetrate a few Angström in the slab (Figure 6G), though no further interstitial migration is observed in the graphite promoted by the presence of fragments.

Initially, the entire lysozyme sequence consists of a single AA chain internally connected by sulfur−sulfur bonds involved in the cysteine residues. When intact lysozymes undergo reactive landing combined with surface-induced dissociation, the changes in the structure can form different amino acid chains in the same protein but not necessarily (Table S3). One example of this is shown in Figure 7A, where three AA chains coexist in the same protein structure after landing. The interruptions in the initial sequence can be due to the removal of oxygen from a C−O bond, damaging the AA structure without breaking the polymeric chain (Figure 7B), or the chain can be connected by two cysteine AA bonds (Figure 7C). Another type of fragmentation reaction is the one that turns an AA into another one, as in the transformation of the sequence from -Tyr-Asp-Thr-Ser-Gly- to -Tyr-Ram-Thr-Gly-Gly- (Figure 7D−G), where Ram is a ramification interconnecting two AAs. In this sequence, the fragmentation of the AA serine

https://doi.org/10.1021/acs.jpcb.4c01698
J. Phys. Chem. B XXXX, XXX, XXX−XXX

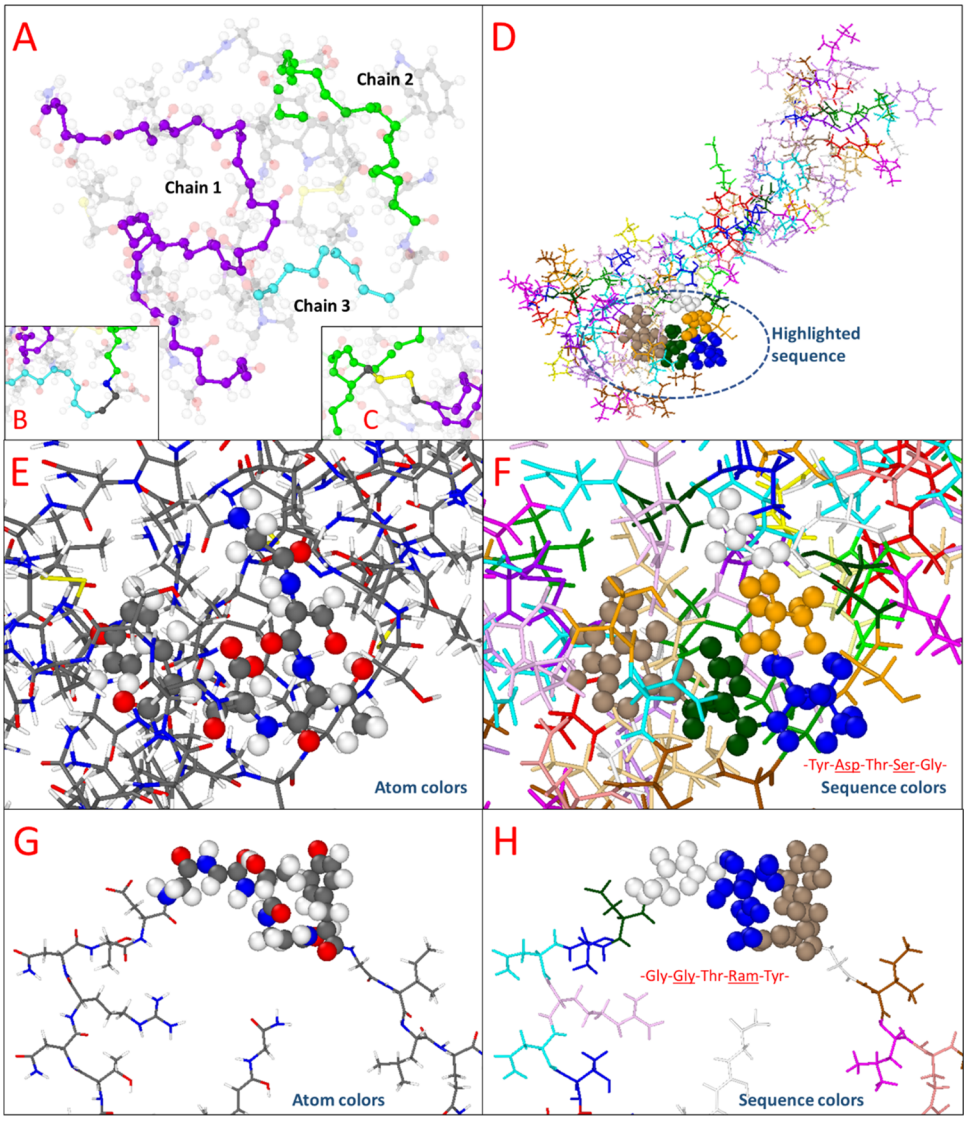

Figure 7. Amino acid sequencing of lysozyme and its fragments. (A) Landed protein where three different chains coexist. (B) Ramification connecting two chains created by the scission of a C−O bond. (C) An S−S bond connects two different amino acids. (D) Isolated lysozyme protein before landing, where a sequence highlighted as balls indicates where it will change after landing. (E) Before landing, the chain region where the protein changes its sequence is colored by atoms, and (F) colored by sequence. (G) After landing, the chain region where the protein changes its sequence colored by atoms and (H) colored by sequence. The fragment that does not belong to any amino acid is hidden, and the ramification (Ram) receives the colors of the connecting amino acids.

transforms it into a glycine, while the break in the asparagine transforms the AA into a non-AA structure containing two carbons but connecting the whole structure.

3.3. Comparison between Gold and HTG Substrates.

As suggested in the previous sections, the substrate's nature influences the landing process. Both substrates are rigid, with Young modulus being ∼80 GPA[88] and ∼1008 GPa[89] for gold and HTG, respectively. Consequently, differences in the landing and/or scattering are mainly governed by the binding energies per unit area after optimization of the protein adsorbed and in a vacuum, which amounts to 3.41×10^{-2} and 0.98×10^{-2} eV/Å^2 for lysozyme adsorbed on gold and HTG, respectively, in our simulations using ReaxFF. In comparison, DFT calculations give adsorption energies for neurotensin of 1.20×10^{-2} eV/Å^2 for gold and 0.25×10^{-2} eV/Å^2 for HTG, while another configuration on gold gives a value of 1.19×10^{-2}, which can be considered a negligible difference. Additionally, the total charge between the substrate and the neurotensin, calculated by DFT methods, shows a higher transference of charge from neurotensin to the slab on gold than in HTG, −1.72 and −1.18 lel, respectively. The charge distribution on the substrate tends to accumulate negative charges on the gold surface atoms, while no clear tendency is observed on HTG (Figure S7C,D).

Even though the absolute values of binding energy are larger for the ReaxFF calculations with lysozyme than the DFT calculations involving neurotensin, the binding energy is much larger on gold in both models (by a factor of ∼4). Although the adsorption energies obtained by DFT for neurotensin can only constitute a crude approximation of our lysozyme systems, the purpose was indeed to confirm the significant difference in adsorption energy of such molecules toward the two substrates. The effect of the substrate's nature is expressed by the sticking coefficient (m_{landed}/m_{total}, the mass of the landed proteins and the total mass of proteins) that varies with the substrate and the collision angle (Table 3). In agreement with

https://doi.org/10.1021/acs.jpcb.4c01698
J. Phys. Chem. B XXXX, XXX, XXX−XXX

Table 3. Sticking Coefficient and Denaturation Ratios of Landed Proteins

substrate	protein configuration	sticking coefficient	denaturation ratio
gold	clustered	1.000	1.720
	oblique	0.784	1.306
	normal	0.964	1.310
graphite	clustered	1.000	0.759
	oblique	0.687	0.652
	normal	0.475	0.815

the higher binding energy, the sticking coefficient tends to be higher for gold than for HTG, on average, and for all impact angles. However, the impact angle also affects the sticking coefficient and in an opposite fashion for gold and HTG. In both cases, the angle-induced variation of the sticking coefficient (Table 3) corresponds to an inverse change in the number of fragments in the gas phase (Figure 2). In our simulations, the total atomic kinetic energy of a protein encompasses its translational, vibrational, and rotational velocities. As collision progresses, the kinetic energy of the lysozymes gradually diminishes over time until it stabilizes at a constant value. Consequently, due to this inelastic impact, the protein imparts energy to the gold slab, which is subsequently dissipated through the Langevin layers within gold or HTG, and a portion of the translational kinetic energy remains with the backscattered fragments (Figure S5). Interestingly, the kinetic energy transferred to the substrate or kept in the system at the end of the collision does not seem to correlate strongly with the angular dependence of the fragmentation or reflection capacity for each substrate (Figure S5A–C). Instead, it appears more influenced by the substrate's nature, certainly for normal impacts (Figure S5B). Therefore, backscattering is induced by the difference in adhesion forces and perhaps, to some extent, by the comparatively higher Young modulus of HTG (as the sticking coefficient for normal impacts).

Another effect of the different attractive forces of the two substrates is visible in the conformation of soft-landed proteins. In the case of gold, the robust electrostatic interactions between the substrate and the proteins cause the proteins to denature and flatten over the surface to maximize interactions, whereas the weaker van der Waals interactions of HTG allow the proteins to better keep their conformation and to migrate

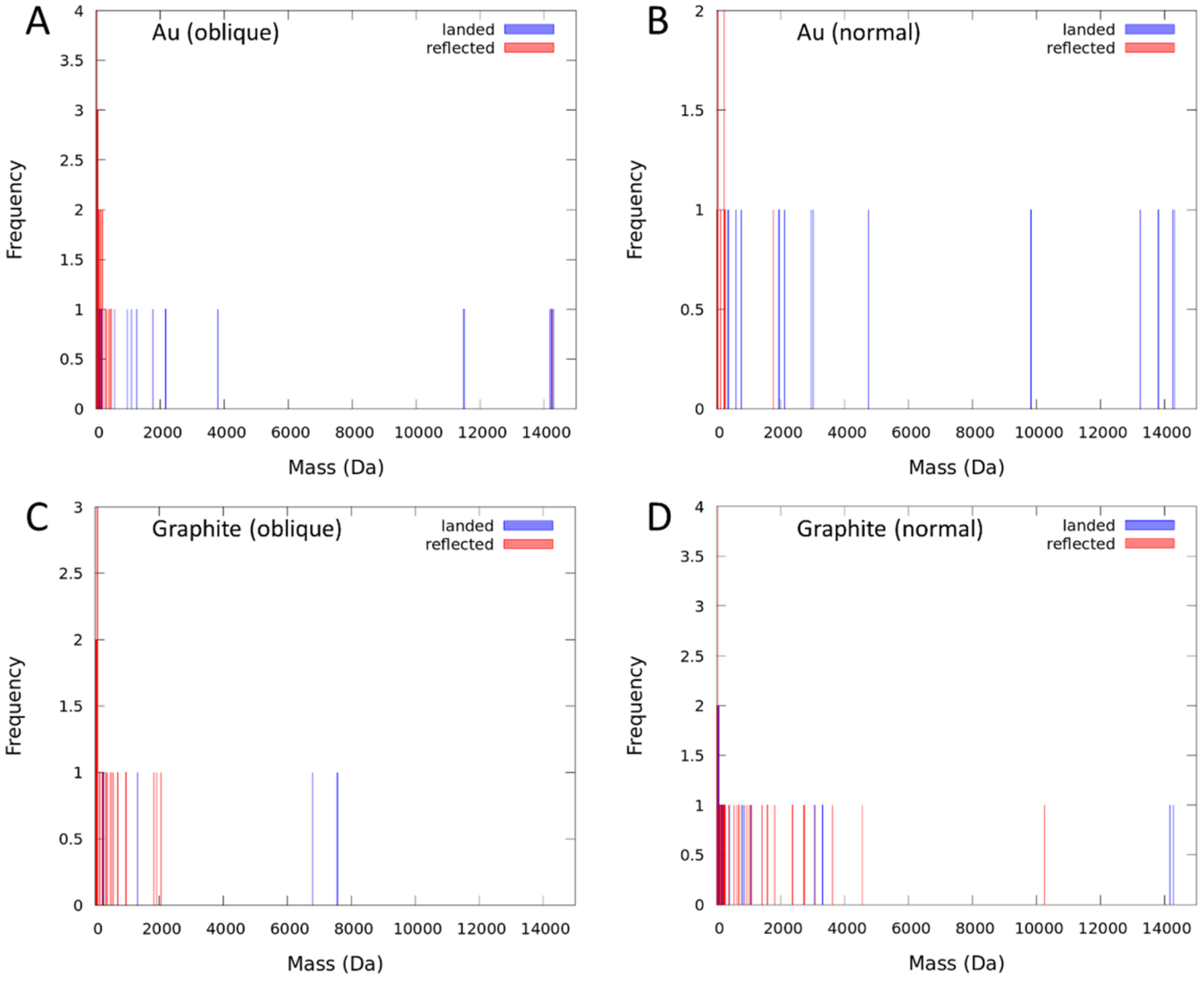

Figure 8. Mass spectrometry of landed proteins on gold and HTG. (A) oblique incidence on gold, (B) normal incidence on gold, (C) oblique incidence on HTG, and (D) normal incidence on HTG.

https://doi.org/10.1021/acs.jpcb.4c01698
J. Phys. Chem. B XXXX, XXX, XXX−XXX

across the surface after landing. For comparison, the total charge of the protein clusters landed on gold and HTG are −347.7 and −16.9 lel, respectively. The denaturation ratio (A_f/A_i, final and initial solvent accessible surface area) also varies based on the substrate's nature and the initial protein structure during flight (Table 3). On gold, the denaturation ratio exceeds 1.0, indicating greater protein unfolding compared to its initial flying state. In contrast, on HTG, the denaturation ratio is below 1.0, suggesting that the proteins compress and revert to a state that is more globular and thereby probably closer to their native state after landing. On HTG, the reduction of the molecular surface area upon landing is slightly more pronounced for the clustered than for isolated proteins upon normal incidence, perhaps indicating that the structuring effect of forces within the group of proteins dominates over the protein−substrate interactions. Additionally, the temperature dragged from the protein to the substrate should influence the denaturation ratio. Conversely, on gold, the increase of the molecular surface area is the highest for the initially clustered proteins, condensing and then spreading across the gold surface, which can be explained by the prevalence of the protein−substrate interactions over the cluster structuring forces (and the intramolecular nonbonding forces supposed to maintain the secondary and tertiary structures of the proteins). An effect of the landing angle of isolated molecules on the denaturation ratio is measurable only for HTG, likely linked to the larger fragmentation computed for normal impacts.

In the case of isolated lysozyme landing, the distribution of molecular masses observed between landed and reflected molecules (Figure 8) indicates first that both intact lysozyme and large fragments can adsorb on both surfaces. Typically, small fragments are predominantly reflected away from the surface, though larger fragments can also be backscattered in some cases. On gold, oblique landing does not seem to result in the reflection of large fragments (while a fragment weighing around 2000 Da is seen in the backscattered flux for normal incidence) and there are also more occurrences of adsorbed larger fragments (>8000 g/mol) for normal impacts. In general, the angle of incidence has a more significant impact on fragment backscattering for HTG substrates, with a comparatively higher number of heavy fragments being reflected from the surface during normal collisions. Overall, the distribution of reflected fragments extends to higher masses for HTG than for gold, regardless of the collision angle. Figure S6 highlights the mass distributions of small fragments (<250 Da). It is noticeable that small fragments are more prevalent in the backscattered than the adsorbed species for both substrates. For gold, the number of small fragments varies with the landing inclination angle, with larger numbers for oblique incidence. Finally, HTG generally yields fewer small fragments compared to the gold substrate

4. DISCUSSION

According to our simulations, protein transfer induced by GCIB can lead to both soft and reactive landing and/or surface-induced dissociation, depending on the desorption conditions. Clusters of lysozymes tend to promote soft landing on both gold and HTG substrates, even though binding of one protein to a C atom of the HTG is observed (Figure S4). In contrast, isolated proteins are more prone to undergoing reactive landing and surface-induced dissociation via fragmentation when reaching the collector. The change in soft to reactive landing is mirrored by the translational and internal energies per unit mass, which are higher for isolated lysozymes than for the protein clusters (Table 1). These clusters were emitted from a thick layer of lysozyme by Ar_{5000} clusters with rather low energy per atom, corresponding to the experimental case where soft landing could be assessed by measuring the bioactivity of the enzymes after landing.[41]

In the desorption process, more fragmented molecules can originate either from hard bombardment conditions (E/n > 10 eV) from a thick organic layer or, with comparatively lower E/n, from a (sub)monolayer adsorbed on a hard substrate like gold. In the latter case, the Ar cluster energy is indeed confined to the surface and the stronger binding of the molecules induces a larger stress upon desorption.[45] This effect of the organic layer thickness was experimentally verified for thin polymeric layers on silicon.[90] Thus, if the target becomes exhausted, proteins will tend to desorb with higher fragmentation and internal kinetic energy, causing further fragmentation upon landing. On the other hand, it can be speculated that, as proteins accumulate on the collector, their behavior during landing might change due to the transition from a rigid to a soft substrate. In this work, both gold and HTG substrates were rigid materials, so that case remains to be investigated. However, our data indicate that proteins landing on other proteins already immobilized on the gold collector tend to be more backscattered. The effect of the collector nature on the final conformation of the landed proteins is clear for both low-energy lysozyme clusters and higher-energy isolated molecules, irrespective of the incidence angle, as indicated by the calculated denaturation ratios. The stronger adhesion forces with the gold substrate induce denaturation, while the lower van der Waals forces of the HTG collector allow the proteins to keep or even recover a conformation that is closer to their native globular state. Similar effects of unfolding and refolding depending on the collector surface nature and the deposition parameters have been experimentally measured by AFM and STM in the case of protein ion soft landing using electrospray.[91]

An extreme case studied in our simulations with HTG substrates is when the proteins are desorbed as fragments by more energetic Ar clusters. In that case, the reactivity is higher, potentially due to the under- or overcoordination of the fragments. While many fragments undergo further rupture and are backscattered from the substrate, a significant number of them establish new bonds with graphite. It is plausible that organic substrates, like polymers, could interact with such fragments, although this might also depend to some extent on the substrate's rigidity. One aspect to be explored in future research is reactivity with soft collector materials, which would also mimic the case of a growing multilayer coating, where the substrate is already covered with a full layer of organic matter.

The iBEAM technique represents an innovative approach to achieving soft and reactive landing. At this stage, in contrast to conventional methods, such as ESI and MALDI, iBEAM does not select charged proteins for landing. Instead, collisions with Ar clusters induce hyperthermal desorption of a majority of neutrals and only a fraction of ions that are all transferred to the collector, yielding less selectivity but much larger deposition rates. Nevertheless, strong similarities exist such as the propensity for proteins with higher internal energy and momentum to undergo surface-induced dissociation. Similar to the other methods, our results show that heavy proteins and their clusters can reactively land on graphite surfaces with the substrate directly influencing the landing process. The main

https://doi.org/10.1021/acs.jpcb.4c01698
J. Phys. Chem. B XXXX, XXX, XXX−XXX

advantages of iBEAM lie in the ability to tune the fragmentation and internal energies of the transferred molecules via the Ar cluster parameters and in the ease of building multilayers with excellent nanoscale thickness control.

5. CONCLUSIONS

Molecular dynamics simulations of soft landing using ReaxFF indicate that proteins like lysozymes desorbed by large Ar clusters (GCIB) can undergo either soft landing or surface-induced dissociation on gold and HTG collectors. The nature of the landing is directly connected to the desorption process from the target and to the substrate where the molecules land, providing experimentalists in the field with a number of parameters to control the quality of the deposited material.

Comparing gold and HTG, the latter tends to induce greater protein fragmentation and backscattering. However, because of stronger adhesion forces, gold causes complete denaturation of the first layer of lysozyme on the substrate, while HTG tends to foster the creation of more spherical protein structures. The landing dynamics is also influenced by the angle of incidence of the proteins on the collector. For example, the collision angle can dictate the number of resulting fragments and the quantity of proteins reflected on the surface. In the conditions of reactive landing and surface-induced dissociation, the observed reactions can be simple protein fragmentations, reactions between the protein and the substrate (for HTG substrates), reactions within the proteins (migration of hydrogen), or reactions between parts of different proteins forming new molecules.

Our computational studies reasonably predict the entire process of molecular transfer and redeposition using large cluster ion beams, from desorption to landing of lysozymes and their noncovalent complexes, suggesting that the method could be successful with larger biomolecules.[43] Interestingly, it also predicts a mechanism by which such hyperthermal velocity proteins can covalently graft on a substrate with minimal damage, a feature that might have significant relevance in technological applications, e.g., for biosensors with improved performance.[92]

■ ASSOCIATED CONTENT

Supporting Information

The Supporting Information is available free of charge at https://pubs.acs.org/doi/10.1021/acs.jpcb.4c01698.

Description of how the in-house code names different proteins; additionally, the Supporting Information encompasses all the complementary images and tables mentioned in the text; the images are used to describe soft and reactive landing and help to describe the simulations (PDF)

■ AUTHOR INFORMATION

Corresponding Author

Samuel Bertolini − *Institute of Condensed Matter and Nanoscience, Université catholique de Louvain, 1348 Louvain-la-Neuve, Belgium;* orcid.org/0000-0003-0969-7142; Email: samuel.bertolini@uclouvain.be

Author

Arnaud Delcorte − *Institute of Condensed Matter and Nanoscience, Université catholique de Louvain, 1348 Louvain-la-Neuve, Belgium;* orcid.org/0000-0003-4127-8650

Complete contact information is available at: https://pubs.acs.org/10.1021/acs.jpcb.4c01698

Notes

The authors declare no competing financial interest.

■ ACKNOWLEDGMENTS

The authors wish to thank the funding organizations that supported the production of this article and the Supporting Information: the "Fonds National de la Recherche Scientifique" (FNRS) for financing the project "Cluster-protein impacts" under the convention PDR T.0052.22 and the additional funding that was provided by the Fédération Wallonie Bruxelles, through the project "iBEAM" (ARC convention No 18/23-090). We also acknowledge the computational resources provided by the Institut de Calcul Intensif et de Stockage de Masse (CISM) at Université catholique de Louvain and the network of high-performance computing of Wallonia (CECI).

■ REFERENCES

(1) Britton, J.; Raston, C. L.; Weiss, G. A. Rapid Protein Immobilization for Thin Film Continuous Flow Biocatalysis. *Chem. Commun.* **2016**, *52* (66), 10159−10162.

(2) Samanta, A.; Stuart, M. C. A.; Ravoo, B. J. Photoresponsive Capture and Release of Lectins in Multilamellar Complexes. *J. Am. Chem. Soc.* **2012**, *134* (48), 19909−19914.

(3) Herr, A. E. Disruptive by Design: A Perspective on Engineering in Analytical Chemistry. *Anal. Chem.* **2013**, *85* (16), 7622−7628.

(4) Samanta, D.; Sarkar, A. Immobilization of Bio-Macromolecules on Self-Assembled Monolayers: Methods and Sensor Applications. *Chem. Soc. Rev.* **2011**, *40* (5), 2567−2592.

(5) Li, T.; Hao, L.; Li, J.; Du, C.; Wang, Y. Insight into Vitronectin Structural Evolution on Material Surface Chemistries: The Mediation for Cell Adhesion. *Bioact. Mater.* **2020**, *5* (4), 1044−1052.

(6) Jain, A.; Trindade, G. F.; Hicks, J. M.; Potts, J. C.; Rahman, R.; Hague, R. J. M.; Amabilino, D. B.; Pérez-García, L.; Rawson, F. J. Modulating the Biological Function of Protein by Tailoring the Adsorption Orientation on Nanoparticles. *J. Colloid Interface Sci.* **2021**, *587*, 150−161.

(7) Absolom, D. R.; Neumann, A. W. Modification of Substrate Surface Properties through Protein Adsorption. *Colloids Surf.* **1987**, *30* (1), 25−45.

(8) Jacquemart, I.; Pamuła, E.; De Cupere, V. M.; Rouxhet, P. G.; Dupont-Gillain, C. C. Nanostructured Collagen Layers Obtained by Adsorption and Drying. *J. Colloid Interface Sci.* **2004**, *278* (1), 63−70.

(9) Denis, F. A.; Pallandre, A.; Nysten, B.; Jonas, A. M.; Dupont-Gillain, C. C. Alignment and Assembly of Adsorbed Collagen Molecules Induced by Anisotropic Chemical Nanopatterns. *Small* **2005**, *1* (10), 984−991.

(10) vander Straeten, A.; Bratek-Skicki, A.; Jonas, A. M.; Fustin, C.-A.; Dupont-Gillain, C. Integrating Proteins in Layer-by-Layer Assemblies Independently of Their Electrical Charge. *ACS Nano* **2018**, *12* (8), 8372−8381.

(11) Vranckx, C.; Lambricht, L.; Préat, V.; Cornu, O.; Dupont-Gillain, C.; vander Straeten, A. Layer-by-Layer Nanoarchitectonics Using Protein−Polyelectrolyte Complexes toward a Generalizable Tool for Protein Surface Immobilization. *Langmuir* **2022**, *38* (18), 5579−5589.

(12) Ott, W.; Durner, E.; Gaub, H. E. Enzyme-Mediated, Site-Specific Protein Coupling Strategies for Surface-Based Binding Assays. *Angew. Chem.* **2018**, *130* (39), 12848−12851.

(13) Wong, L. S.; Khan, F.; Micklefield, J. Selective Covalent Protein Immobilization: Strategies and Applications. *Chem. Rev.* **2009**, *109* (9), 4025−4053.
(14) Jung, Y.; Jeong, J. Y.; Chung, B. H. Recent Advances in Immobilization Methods of Antibodies on Solid Supports. *Analyst* **2008**, *133* (6), 697−701.
(15) Cooks, R. G.; Yan, X. Mass Spectrometry for Synthesis and Analysis. *Annu. Rev. Anal. Chem.* **2018**, *11*, 1−28, DOI: 10.1146/annurev-anchem-061417-125820.
(16) Washburn, M. P. Soft Landing for Protein Chips. *Nat. Biotechnol.* **2003**, *21* (10), 1156−1157.
(17) Gologan, B.; Takáts, Z.; Alvarez, J.; Wiseman, J. M.; Talaty, N.; Ouyang, Z.; Cooks, R. G. Ion Soft-Landing into Liquids: Protein Identification, Separation, and Purification with Retention of Biological Activity. *J. Am. Soc. Mass Spectrom.* **2004**, *15* (12), 1874−1884.
(18) Passarelli, M. K.; Pirkl, A.; Moellers, R.; Grinfeld, D.; Kollmer, F.; Havelund, R.; Newman, C. F.; Marshall, P. S.; Arlinghaus, H.; Alexander, M. R.; West, A.; Horning, S.; Niehuis, E.; Makarov, A.; Dollery, C. T.; Gilmore, I. S. The 3D OrbiSIMS—Label-Free Metabolic Imaging with Subcellular Lateral Resolution and High Mass-Resolving Power. *Nat. Methods* **2017**, *14* (12), 1175−1183.
(19) Gologan, B.; Green, J. R.; Alvarez, J.; Laskin, J.; Cooks, R. G. Ion/Surface Reactions and Ion Soft-Landing. *Phys. Chem. Chem. Phys.* **2005**, *7* (7), 1490−1500.
(20) Volný, M.; Elam, W. T.; Branca, A.; Ratner, B. D.; Tureček, F. Preparative Soft and Reactive Landing of Multiply Charged Protein Ions on a Plasma-Treated Metal Surface. *Anal. Chem.* **2005**, *77* (15), 4890−4896.
(21) Blacken, G. R.; Volný, M.; Diener, M.; Jackson, K. E.; Ranjitkar, P.; Maly, D. J.; Tureček, F. Reactive Landing of Gas-Phase Ions as a Tool for the Fabrication of Metal Oxide Surfaces for in Situ Phosphopeptide Enrichment. *J. Am. Soc. Mass Spectrom.* **2009**, *20* (6), 915−926.
(22) Benesch, J. L. P.; Ruotolo, B. T.; Simmons, D. A.; Robinson, C. V. Protein Complexes in the Gas Phase: Technology for Structural Genomics and Proteomics. *Chem. Rev.* **2007**, *107* (8), 3544−3567.
(23) Ouyang, Z.; Takáts, Z.; Blake, T. A.; Gologan, B.; Guymon, A. J.; Wiseman, J. M.; Oliver, J. C.; Davisson, V. J.; Cooks, R. G. Preparing Protein Microarrays by Soft-Landing of Mass-Selected Ions. *Science* **2003**, *301* (5638), 1351−1354.
(24) Guo, H.; Jiang, B. The Sudden Vector Projection Model for Reactivity: Mode Specificity and Bond Selectivity Made Simple. *Acc. Chem. Res.* **2014**, *47* (12), 3679−3685.
(25) Harvey, S. R.; Seffernick, J. T.; Quintyn, R. S.; Song, Y.; Ju, Y.; Yan, J.; Sahasrabuddhe, A. N.; Norris, A.; Zhou, M.; Behrman, E. J.; Lindert, S.; Wysocki, V. H. Relative Interfacial Cleavage Energetics of Protein Complexes Revealed by Surface Collisions. *Proc. Natl. Acad. Sci. U.S.A.* **2019**, *116* (17), 8143−8148.
(26) Krumbein, L.; Anggara, K.; Stella, M.; Michnowicz, T.; Ochner, H.; Abb, S.; Rinke, G.; Portz, A.; Dürr, M.; Schlickum, U.; Baldwin, A.; Floris, A.; Kern, K.; Rauschenbach, S. Fast Molecular Compression by a Hyperthermal Collision Gives Bond-Selective Mechanochemistry. *Phys. Rev. Lett.* **2021**, *126* (5), 56001.
(27) Bartels, N.; Golibrzuch, K.; Bartels, C.; Chen, L.; Auerbach, D. J.; Wodtke, A. M.; Schäfer, T. Observation of Orientation-Dependent Electron Transfer in Molecule−Surface Collisions. *Proc. Natl. Acad. Sci. U.S.A.* **2013**, *110* (44), 17738−17743.
(28) Kramer, K. H.; Bernstein, R. B. Focusing and Orientation of Symmetric-Top Molecules with the Electric Six-Pole Field. *J. Chem. Phys.* **1965**, *42* (2), 767−770.
(29) Esser, T. K.; Böhning, J.; Önür, A.; Chinthapalli, D. K.; Eriksson, L.; Grabarics, M.; Fremdling, P.; Konijnenberg, A.; Makarov, A.; Botman, A.; Peter, C.; Benesch, J. L. P.; Robinson, C. V.; Gault, J.; Baker, L.; Bharat, T. A. M.; Rauschenbach, S. Cryo-EM of Soft-Landed β-Galactosidase: Gas-Phase and Native Structures Are Remarkably Similar. *Sci. Adv.* **2024**, *10* (7), No. eadl4628.
(30) Barth, J. V. Molecular Architectonic on Metal Surfaces. *Annu. Rev. Phys. Chem.* **2007**, *58* (Volume 58, 2007), 375−407.
(31) Hadjar, O.; Futrell, J. H.; Laskin, J. First Observation of Charge Reduction and Desorption Kinetics of Multiply Protonated Peptides Soft Landed onto Self-Assembled Monolayer Surfaces. *J. Phys. Chem. C* **2007**, *111* (49), 18220−18225.
(32) Badman, E. R.; Myung, S.; Clemmer, D. E. Evidence for Unfolding and Refolding of Gas-Phase Cytochrome c Ions in a Paul Trap. *J. Am. Soc. Mass Spectrom.* **2005**, *16* (9), 1493−1497.
(33) Ghosh, J.; Cooks, R. G. Mass Spectrometry in Materials Synthesis. *TrAC, Trends Anal. Chem.* **2023**, *161*, No. 117010.
(34) Tata, A.; Salvitti, C.; Pepi, F. From Vacuum to Atmospheric Pressure: A Review of Ambient Ion Soft Landing. *Int. J. Mass Spectrom.* **2020**, *450*, No. 116309.
(35) Westphall, M. S.; Lee, K. W.; Salome, A. Z.; Lodge, J.; Grant, T.; Coon, J. J.3D Structure Determination of Protein Complexes Using Matrix-Landing Mass Spectrometry *bioRxiv* 2021; Vol. *2021*, p 2021-10 DOI: 10.1101/2021.10.13.464253.
(36) Lee, K. W.; Salome, A. Z.; Westphall, M. S.; Grant, T.; Coon, J. J. Onto Grid Purification and 3D Reconstruction of Protein Complexes Using Matrix-Landing Native Mass Spectrometry. *J. Proteome Res.* **2023**, *22* (3), 851−856.
(37) Laskin, J.; Futrell, J. H. Surface-Induced Dissociation of Peptide Ions: Kinetics and Dynamics. *J. Am. Soc. Mass Spectrom.* **2003**, *14* (12), 1340−1347.
(38) McCabe, J. W.; Shirzadeh, M.; Walker, T. E.; Lin, C.-W.; Jones, B. J.; Wysocki, V. H.; Barondeau, D. P.; Clemmer, D. E.; Laganowsky, A.; Russell, D. H. Variable-Temperature Electrospray Ionization for Temperature-Dependent Folding/Refolding Reactions of Proteins and Ligand Binding. *Anal. Chem.* **2021**, *93* (18), 6924−6931.
(39) Laskin, J.; Bailey, T. H.; Futrell, J. H. Shattering of Peptide Ions on Self-Assembled Monolayer Surfaces. *J. Am. Chem. Soc.* **2003**, *125* (6), 1625−1632.
(40) Delcorte, A.; Delmez, V.; Dupont-Gillain, C.; Lauzin, C.; Jefford, H.; Chundak, M.; Poleunis, C.; Moshkunov, K. Large Cluster Ions: Soft Local Probes and Tools for Organic and Bio Surfaces. *Phys. Chem. Chem. Phys.* **2020**, *22* (31), 17427−17447.
(41) Delmez, V.; Degand, H.; Poleunis, C.; Moshkunov, K.; Chundak, M.; Dupont-Gillain, C.; Delcorte, A. Deposition of Intact and Active Proteins In Vacuo Using Large Argon Cluster Ion Beams. *J. Phys. Chem. Lett.* **2021**, *12* (2), 952−957.
(42) Delmez, V.; Tomasetti, B.; Daphnis, T.; Poleunis, C.; Lauzin, C.; Dupont-Gillain, C.; Delcorte, A. Gas Cluster Ion Beams as a Versatile Soft-Landing Tool for the Controlled Construction of Thin (Bio) Films. *ACS Appl. Bio Mater.* **2022**, *5* (7), 3180−3192.
(43) Bertolini, S.; Delcorte, A. Unraveling the Molecular Dynamics of Glucose Oxidase Desorption Induced by Argon Cluster Collision. *J. Phys. Chem. B* **2023**, *127* (42), 9074−9081.
(44) Fu, T.; Della-Negra, S.; Touboul, D.; Brunelle, A. Internal Energy Distribution of Secondary Ions under Argon and Bismuth Cluster Bombardments:"Soft" versus "Hard" Desorption−Ionization Process. *J. Am. Soc. Mass Spectrom.* **2019**, *30* (2), 321−328.
(45) Bertolini, S.; Delcorte, A. Reactive Molecular Dynamics Simulations of Lysozyme Desorption under Ar Cluster Impact. *Appl. Surf. Sci.* **2023**, *631*, 157487 DOI: 10.1016/j.apsusc.2023.157487.
(46) Westphall, M. S.; Lee, K. W.; Hemme, C.; Salome, A. Z.; Mertz, K.; Grant, T.; Coon, J. J. Cryogenic Soft Landing Improves Structural Preservation of Protein Complexes. *Anal. Chem.* **2023**, *95* (40), 15094−15101.
(47) Esser, T. K.; Böhning, J.; Önür, A.; Chinthapalli, D. K.; Eriksson, L.; Grabarics, M.; Fremdling, P.; Konijnenberg, A.; Makarov, A.; Botman, A.; Peter, C.; Benesch, J. L. P.; Robinson, C. V.; Gault, J.; Baker, L.; Bharat, T. A. M.; Rauschenbach, S. Cryo-EM of soft-landed β-galactosidase: Gas-phase and native structures are remarkably similar. *Sci. Adv.* **2024**, *10* (7), eadl4628 DOI: 10.1101/2023.08.17.553673.
(48) Delcorte, A. A Microscopic View of Macromolecule Transfer in the Vacuum Using Gas and Bismuth Clusters. *J. Phys. Chem. C* **2022**, *126* (16), 7307−7318.

(49) Paruch, R. J.; Postawa, Z.; Garrison, B. J. Seduction of Finding Universality in Sputtering Yields Due to Cluster Bombardment of Solids. *Acc. Chem. Res.* **2015**, *48* (9), 2529−2536.
(50) Garrison, B. J.; Postawa, Z. Computational View of Surface Based Organic Mass Spectrometry. *Mass Spectrom. Rev.* **2008**, *27* (4), 289−315.
(51) Postawa, Z.; Czerwinski, B.; Szewczyk, M.; Smiley, E. J.; Winograd, N.; Garrison, B. J. Microscopic Insights into the Sputtering of Ag{111} Induced by C60 and Ga Bombardment. *J. Phys. Chem. B* **2004**, *108* (23), 7831−7838.
(52) Anggara, K.; Zhu, Y.; Delbianco, M.; Rauschenbach, S.; Abb, S.; Seeberger, P. H.; Kern, K. Exploring the Molecular Conformation Space by Soft Molecule−Surface Collision. *J. Am. Chem. Soc.* **2020**, *142* (51), 21420−21427.
(53) Anggara, K.; Ochner, H.; Szilagyi, S.; Malavolti, L.; Rauschenbach, S.; Kern, K. Landing Proteins on Graphene Trampoline Preserves Their Gas-Phase Folding on the Surface. *ACS Cent. Sci.* **2023**, *9* (2), 151−158.
(54) Frederickson, D.; McDonough, M.; Barnes, G. L. A Computational Comparison of Soft Landing of α-Helical vs Globular Peptides. *J. Phys. Chem. B* **2018**, *122* (41), 9549−9554.
(55) Martin Somer, A.; Macaluso, V.; Barnes, G. L.; Yang, L.; Pratihar, S.; Song, K.; Hase, W. L.; Spezia, R. Role of Chemical Dynamics Simulations in Mass Spectrometry Studies of Collision-Induced Dissociation and Collisions of Biological Ions with Organic Surfaces. *J. Am. Soc. Mass Spectrom.* **2020**, *31* (1), 2−24.
(56) Pratihar, S.; Kohale, S. C.; Bhakta, D. G.; Laskin, J.; Hase, W. L. Dynamics of Energy Transfer and Soft-Landing in Collisions of Protonated Dialanine with Perfluorinated Self-Assembled Monolayer Surfaces. *Phys. Chem. Chem. Phys.* **2014**, *16* (43), 23769−23778.
(57) Gu, M.; Yang, L.; Hase, W. L.; Sun, J.; Zhang, J. Energy Transfer of Peptide Ions Colliding with a Self-Assembled Monolayer Surface. The Influence of Peptide Ion Size. *Chin. J. Chem.* **2019**, *37* (3), 237−243.
(58) Barnes, G. L.; Hase, W. L. Energy Transfer, Unfolding, and Fragmentation Dynamics in Collisions of N-Protonated Octaglycine with an H-SAM Surface. *J. Am. Chem. Soc.* **2009**, *131* (47), 17185−17193.
(59) Pratihar, S.; Barnes, G. L.; Laskin, J.; Hase, W. L. Dynamics of Protonated Peptide Ion Collisions with Organic Surfaces: Consonance of Simulation and Experiment. *J. Phys. Chem. Lett.* **2016**, *7* (16), 3142−3150.
(60) Barnes, G. L.; Young, K.; Yang, L.; Hase, W. L. Fragmentation and Reactivity in Collisions of Protonated Diglycine with Chemically Modified Perfluorinated Alkylthiolate-Self-Assembled Monolayer Surfaces. *J. Chem. Phys.* **2011**, *134* (9), 094106 DOI: 10.1063/1.3558736.
(61) Wang, P.; Hadjar, O.; Laskin, J. Covalent Immobilization of Peptides on Self-Assembled Monolayer Surfaces Using Soft-Landing of Mass-Selected Ions. *J. Am. Chem. Soc.* **2007**, *129* (28), 8682−8683.
(62) Wang, P.; Hadjar, O.; Gassman, P. L.; Laskin, J. Reactive Landing of Peptide Ions on Self-Assembled Monolayer Surfaces: An Alternative Approach for Covalent Immobilization of Peptides on Surfaces. *Phys. Chem. Chem. Phys.* **2008**, *10* (11), 1512−1522.
(63) Hanley, L.; Sinnott, S. B. The Growth and Modification of Materials via Ion−Surface Processing. *Surf. Sci.* **2002**, *500* (1−3), 500−522.
(64) Hu, Y.; Sinnott, S. B. A Molecular Dynamics Study of Thin-Film Formation via Molecular Cluster Beam Deposition: Effect of Incident Species. *Surf. Sci.* **2003**, *526* (3), 230−242.
(65) Hsu, W.-D.; Tepavcevic, S.; Hanley, L.; Sinnott, S. B. Mechanistic Studies of Surface Polymerization by Ion-Assisted Deposition. *J. Phys. Chem. C* **2007**, *111* (11), 4199−4208.
(66) Zarshenas, M.; Moshkunov, K.; Czerwinski, B.; Leyssens, T.; Delcorte, A. Molecular Dynamics Simulations of Hydrocarbon Film Growth from Acetylene Monomers and Radicals: Effect of Substrate Temperature. *J. Phys. Chem. C* **2018**, *122* (27), 15252−15263.
(67) Kański, M.; Maciążek, D.; Postawa, Z.; Ashraf, C. M.; van Duin, A. C. T.; Garrison, B. J. Development of a Charge-Implicit ReaxFF Potential for Hydrocarbon Systems. *J. Phys. Chem. Lett.* **2018**, *9* (2), 359−363.
(68) Senftle, T. P.; Hong, S.; Islam, M. M.; Kylasa, S. B.; Zheng, Y.; Shin, Y. K.; Junkermeier, C.; Engel-Herbert, R.; Janik, M. J.; Aktulga, H. M.; et al. The ReaxFF Reactive Force-Field: Development, Applications and Future Directions. *NPJ Comput. Mater.* **2016**, *2* (1), 1−14.
(69) Van Duin, A. C. T.; Dasgupta, S.; Lorant, F.; Goddard, W. A. ReaxFF: A Reactive Force Field for Hydrocarbons. *J. Phys. Chem. A* **2001**, *105* (41), 9396−9409.
(70) Kanski, M.; Garrison, B. J.; Postawa, Z. Effect of Oxygen Chemistry in Sputtering of Polymers. *J. Phys. Chem. Lett.* **2016**, *7* (8), 1559−1562.
(71) Gołuński, M.; Hrabar, S.; Postawa, Z. Mechanisms of Molecular Emission from Phenylalanine Monolayer Deposited on Free-Standing Graphene Bombarded by C60 Projectiles. *Appl. Surf. Sci.* **2021**, *539*, No. 148259.
(72) Mücksch, C.; Anders, C.; Gnaser, H.; Urbassek, H. M. Dynamics of L-Phenylalanine Sputtering by Argon Cluster Bombardment. *J. Phys. Chem. C* **2014**, *118* (15), 7962−7970.
(73) Islam, M. M.; Kolesov, G.; Verstraelen, T.; Kaxiras, E.; Van Duin, A. C. T. EReaxFF: A Pseudoclassical Treatment of Explicit Electrons within Reactive Force Field Simulations. *J. Chem. Theory Comput.* **2016**, *12* (8), 3463−3472.
(74) Islam, M. M.; Van Duin, A. C. T. Reductive Decomposition Reactions of Ethylene Carbonate by Explicit Electron Transfer from Lithium: An EReaxFF Molecular Dynamics Study. *J. Phys. Chem. C* **2016**, *120* (48), 27128−27134.
(75) Bertolini, S.; Jacob, T. Valence Energy Correction for Electron Reactive Force Field. *J. Comput. Chem.* **2022**, *43* (12), 870−878.
(76) Kański, M.; Maciazek, D.; Postawa, Z.; Ashraf, C. M.; Van Duin, A. C. T.; Garrison, B. J. Development of a Charge-Implicit ReaxFF Potential for Hydrocarbon Systems. *J. Phys. Chem. Lett.* **2018**, *9* (2), 359−363.
(77) Alvarez, J.; Cooks, R. G.; Barlow, S. E.; Gaspar, D. J.; Futrell, J. H.; Laskin, J. Preparation and in Situ Characterization of Surfaces Using Soft Landing in a Fourier Transform Ion Cyclotron Resonance Mass Spectrometer. *Anal. Chem.* **2005**, *77* (11), 3452−3460.
(78) Tsai, P. L.; Chen, S.-F.; Huang, S. Y. Mass spectrometry-based strategies for protein disulfide bond identification. *Rev. Anal. Chem.* **2013**, *32* (4), 257−268, DOI: 10.1515/revac-2013-0011.
(79) Thompson, A. P.; Aktulga, H. M.; Berger, R.; Bolintineanu, D. S.; Brown, W. M.; Crozier, P. S.; in 't Veld, P. J.; Kohlmeyer, A.; Moore, S. G.; Nguyen, T. D.; Shan, R.; Stevens, M. J.; Tranchida, J.; Trott, C.; Plimpton, S. J. LAMMPS - a Flexible Simulation Tool for Particle-Based Materials Modeling at the Atomic, Meso, and Continuum Scales. *Comput. Phys. Commun.* **2022**, *271*, No. 108171.
(80) Aktulga, H. M.; Knight, C.; Coffman, P.; O'Hearn, K. A.; Shan, T.-R.; Jiang, W. Optimizing the Performance of Reactive Molecular Dynamics Simulations for Many-Core Architectures. *Int. J. High Perform Comput. Appl.* **2019**, *33* (2), 304−321.
(81) Aktulga, H. M.; Fogarty, J. C.; Pandit, S. A.; Grama, A. Y. Parallel Reactive Molecular Dynamics: Numerical Methods and Algorithmic Techniques. *Parallel Comput.* **2012**, *38* (4−5), 245−259, DOI: 10.1016/j.parco.2011.08.005.
(82) Zhang, W.; Van Duin, A. C. T. Improvement of the ReaxFF Description for Functionalized Hydrocarbon/Water Weak Interactions in the Condensed Phase. *J. Phys. Chem. B* **2018**, *122* (14), 4083−4092.
(83) Monti, S.; Carravetta, V.; Ågren, H. Simulation of Gold Functionalization with Cysteine by Reactive Molecular Dynamics. *J. Phys. Chem. Lett.* **2016**, *7* (2), 272−276.
(84) Kamat, A. M.; Van Duin, A. C. T.; Yakovlev, A. Molecular Dynamics Simulations of Laser-Induced Incandescence of Soot Using an Extended ReaxFF Reactive Force Field. *J. Phys. Chem. A* **2010**, *114* (48), 12561−12572.
(85) Giannozzi, P.; Baroni, S.; Bonini, N.; Calandra, M.; Car, R.; Cavazzoni, C.; Ceresoli, D.; Chiarotti, G. L.; Cococcioni, M.; Dabo, I.; et al. QUANTUM ESPRESSO: A Modular and Open-Source

Software Project for Quantum Simulations of Materials. *J. Phys.: Condens. Matter* **2009**, *21* (39), No. 395502.
(86) Giannozzi, P.; Andreussi, O.; Brumme, T.; Bunau, O.; Nardelli, M. B.; Calandra, M.; Car, R.; Cavazzoni, C.; Ceresoli, D.; Cococcioni, M.; et al. Advanced Capabilities for Materials Modelling with Quantum ESPRESSO. *J. Phys.: Condens. Matter* **2017**, *29* (46), No. 465901.
(87) Tang, W.; Sanville, E.; Henkelman, G. A Grid-Based Bader Analysis Algorithm without Lattice Bias. *J. Phys.: Condens.Matter* **2009**, *21* (8), 084204 DOI: 10.1088/0953-8984/21/8/084204.
(88) Baek, C.-W.; Kim, Y.-K.; Ahn, Y.; Kim, Y.-H. Measurement of the Mechanical Properties of Electroplated Gold Thin Films Using Micromachined Beam Structures. *Sens. Actuators, A* **2005**, *117* (1), 17−27, DOI: 10.1016/j.sna.2003.11.041.
(89) Yu, M.-F.; Files, B. S.; Arepalli, S.; Ruoff, R. S. Tensile Loading of Ropes of Single Wall Carbon Nanotubes and Their Mechanical Properties. *Phys. Rev. Lett.* **2000**, *84* (24), 5552.
(90) Cristaudo, V.; Poleunis, C.; Laha, P.; Eloy, P.; Hauffman, T.; Terryn, H.; Delcorte, A. Ion Yield Enhancement at the Organic/Inorganic Interface in SIMS Analysis Using Ar-GCIB. *Appl. Surf. Sci.* **2021**, *536*, No. 147716.
(91) Rauschenbach, S.; Ternes, M.; Harnau, L.; Kern, K. Mass Spectrometry as a Preparative Tool for the Surface Science of Large Molecules. *Annu. Rev. Anal. Chem.* **2016**, *9* (1), 473−498, DOI: 10.1146/annurev-anchem-071015-041633.
(92) Castrovilli, M. C.; Tempesta, E.; Cartoni, A.; Plescia, P.; Bolognesi, P.; Chiarinelli, J.; Calandra, P.; Cicco, N.; Verrastro, M. F.; Centonze, D.; Gullo, L.; Del Giudice, A.; Galantini, L.; Avaldi, L. Fabrication of a New, Low-Cost, and Environment-Friendly Laccase-Based Biosensor by Electrospray Immobilization with Unprecedented Reuse and Storage Performances. *ACS Sustainable Chem. Eng.* **2022**, *10* (5), 1888−1898.

https://doi.org/10.1021/acs.jpcb.4c01698
J. Phys. Chem. B XXXX, XXX, XXX−XXX